nature neuroscience

Synchronized retinal oscillations encode essential information for escape behavior in frogs

Hiroshi Ishikane[1,2], Mie Gangi[1], Shoko Honda[1] & Masao Tachibana[1]

Synchronized oscillatory activity is generated among visual neurons in a manner that depends on certain key features of visual stimulation. Although this activity may be important for perceptual integration, its functional significance has yet to be explained. Here we find a very strong correlation between synchronized oscillatory activity in a class of frog retinal ganglion cells (dimming detectors) and a well-known escape response, as shown by behavioral tests and multi-electrode recordings from isolated retinas. Escape behavior elicited by an expanding dark spot was suppressed and potentiated by intraocular injection of $GABA_A$ receptor and $GABA_C$ receptor antagonists, respectively. Changes in escape behavior correlated with antagonist-evoked changes in synchronized oscillatory activity but not with changes in the discharge rate of dimming detectors. These antagonists did not affect the expanding dark spot–induced responses in retinal ganglion cells other than dimming detectors. Thus, synchronized oscillations in the retina are likely to encode escape-related information in frogs.

Synchronized activity accompanied by γ-range (~20 to ~80 Hz) oscillations is frequently observed in various nervous systems, and this neural activity may be related to perception, attention and memory[1–13]. In the visual system, synchronized oscillatory activity is found in various regions, such as the retina[14,15], the lateral geniculate nucleus[14,15], the primary visual cortex[1,2,16] and the posteromedial lateral suprasylvian sulcus[17]. Furthermore, synchronized oscillatory activity is found not only among neurons located within one region but also among neurons in different regions[17,18]. The synchronized oscillatory activity depends on certain stimulus features such as continuity and direction of motion[2,19,20], and thus it may serve to integrate spatially distributed features[1,2,14,15,21,22]. However, its functional significance remains unclear.

Frogs jump away when a predator approaches, and the characteristic stimulus that elicits escape behavior is a looming or expanding dark object[23,24]. In the frog retina, ganglion cells are categorized into four classes on the basis of their response properties: sustained contrast detectors, net convexity detectors, moving-edge detectors and dimming detectors[25]. A large darkening or dimming light evokes off-sustained spike discharges in the dimming detector but elicits only a few spike discharges transiently in other cell classes (the non-dimming detector classes)[25]. Of these cell classes, the dimming detectors are of note, as it has been reported that pharmacological blockade of their activity selectively suppresses escape behavior without affecting prey-catching behavior[24]. However, it is not evident how dimming detectors encode escape-related information, although coding by discharge rate is commonly assumed. A possible candidate is synchronized oscillatory spike discharge, which is generated among dimming detectors when a large retinal area is stimulated by a dimming light[26].

As we have already shown in the frog retina, the γ-range oscillations induced in dimming detectors by a large dimming stimulus are suppressed by a $GABA_A$ receptor ($GABA_AR$) antagonist, bicuculline[26,27], whereas these activities are enhanced by a $GABA_CR$ antagonist, (1,2,5,6-tetrahydropyridin-4-yl)methylphosphinic acid (TPMPA)[27]. In the present study, using these GABAR antagonists as a tool, we examined the relationship between visually guided behaviors and light-evoked spike discharges of ganglion cells in isolated retinas. Our results indicate that synchronized oscillatory activity among retinal dimming detectors may have an important role in escape-related visual information processing in frogs.

RESULTS

Suppression of escape behavior by a $GABA_AR$ antagonist

An expanding dark spot that emulated the shadow of an approaching predator evoked escape behavior in frogs (**Fig. 1a**). The escape rate (number of escape trials / total number of trials) increased with increasing expansion speed (**Fig. 1b**; final spot diameter, 55°) and final diameter (**Fig. 1c**; expansion speed, 43° s^{-1}) of the dark spot. When we presented a dark spot expanding from 0° to 55° at a speed of 43° s^{-1}, the escape rate reached ~0.85 (**Fig. 1c**), and the reaction time for escape was 1.01 ± 0.03 s (mean ± s.e.m., $n = 5$ frogs) from the start of spot expansion. Notably, escape behavior was elicited neither by an expanding bright spot nor by an expanding dark ring ($n = 3$ frogs), stimuli which activate the non-dimming detector classes[25] (see **Supplementary Fig. 1** online). These behavioral tests support

[1]Department of Psychology, Graduate School of Humanities and Sociology, The University of Tokyo, 7-3-1 Hongo, Bunkyo-ku, Tokyo 113-0033, Japan. [2]Present address: Laboratory for Neuroinformatics, RIKEN Brain Science Institute, 2-1 Hirosawa, Wako-shi, Saitama 351-0198, Japan. Correspondence should be addressed to M.T. (Ltmasao@L.u-tokyo.ac.jp).

Published online 3 July 2005; doi:10.1038/nn1497

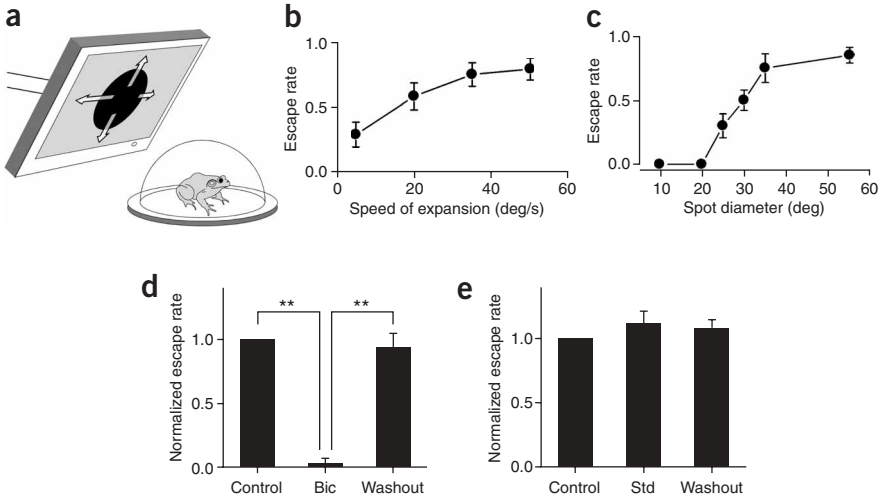

Figure 1 Bicuculline suppressed escape behavior in response to the expanding dark spot. (**a**) Visually elicited escape behavior of a frog was examined with an expanding dark spot presented on a computer-controlled display. (**b**) Relationship between the expansion speed of a dark spot and the escape rate (mean ± s.e.m., $n = 6$ frogs). (**c**) Relationship between the final diameter of an expanding dark spot and the escape rate (mean ± s.e.m., $n = 5$ frogs). (**d**) Suppression of escape behavior by intraocular injection of a $GABA_AR$ antagonist, bicuculline. Behavioral experiments were performed before (Control), 2 h after ('Bic') and 1 d after (Washout) injection. The dark spot expanded from 0° to 55° at the expansion speed of 43° s^{-1}. The escape rate was normalized to the value obtained before injection (Control). Mean ± s.e.m., $n = 5$ frogs. $^{**}P < 0.01$. (**e**) Effect of intraocular injection of the standard saline without bicuculline (mean ± s.e.m., $n = 5$ frogs). The experimental procedure was the same as that employed in **d**.

the hypothesis that dimming detectors may be critical in eliciting escape behavior[24].

The oscillatory discharges that are evoked by a large dimming stimulus in dimming detectors of frog's retinas are suppressed by $GABA_AR$ antagonists[26,27]. Thus, we injected bicuculline into both eyes under anesthesia and allowed the frogs to recover (~2 h). We tested escape behavior with an optimal expanding dark spot (expansion speed, 43° s^{-1}; final spot diameter, 55°; **Fig. 1b**,**c**). This pharmacological treatment significantly suppressed escape behavior ($P < 0.01$, repeated-measures ANOVA followed by Tukey's method, $n = 5$ frogs; **Fig. 1d**). The suppressive effect of bicuculline was recovered 1 d after bicuculline injection (**Fig. 1d**). Intraocular injection of physiological saline without bicuculline did not change escape behavior ($P = 0.46$, repeated-measures ANOVA, $n = 5$ frogs; **Fig. 1e**), indicating that suppression of escape behavior (**Fig. 1d**) could not be ascribed to experimental artifacts such as the effect of anesthesia.

Effects of bicuculline on retinal ganglion cells

To examine how bicuculline affected the responses induced by the expanding dark spot in retinal ganglion cells, we recorded spike discharges extracellularly from isolated frog retinas. Each ganglion cell class was identified as follows: cells that generated off-sustained spike discharges to a full-field stimulus (>4 mm in diameter on the retina) were identified as dimming detectors, cells that generated transient spike discharges at the onset and offset of the full-field stimulus as moving-edge detectors, and cells that evoked transient spike discharges to a small flashing spot (~100 μm in diameter) but no spike discharges to the full-field stimulus as sustained contrast and/or net convexity detectors. The sustained contrast and/or net convexity detectors were categorized as one group because these cells respond similarly to a moving dark stimulus[28]. We stimulated the retinas repeatedly (100 times) with the expanding dark spot, the parameters of which were similar to those used for the behavioral test (from 0° to 60° at the speed of 43° s^{-1}; **Fig. 1d**). We recorded spike discharges from various cell classes, the receptive fields of which were located within the stimulated area. Then we constructed peristimulus time histograms (PSTHs, 50-ms bin width) and autocorrelograms (2-ms bin width) to analyze the temporal pattern of spike discharges (**Fig. 2**).

Dimming detectors generated sustained discharges to the expanding dark spot (**Fig. 2a**, top). Autocorrelation analysis showed a pattern with periodic peaks at regular intervals. The power spectrum, which is the Fourier transform of the autocorrelation function, showed a clear peak at 32.15 ± 1.28 Hz (mean ± s.e.m., $n = 13$ cells), indicating the presence of γ-range oscillations. Bicuculline suppressed the periodic peaks in the autocorrelogram and the peak in the γ range (**Fig. 2a**, bottom), indicating the suppression of γ-range oscillations.

Both sustained contrast and/or net convexity detectors and moving-edge detectors evoked transient discharges to the expanding dark spot (1.73 ± 0.42 spikes/trial in 11 sustained contrast and/or net convexity detectors and 2.72 ± 0.46 spikes/trial in 14 moving edge detectors; **Fig. 2b**,**c**, top). The autocorrelograms and power spectra do not indicate any detectable γ-range oscillations in these non-dimming detector classes (**Fig. 2b**,**c**). Bicuculline did not induce any obvious changes in the profiles of PSTHs, autocorrelograms or power spectra (**Fig. 2b**,**c**, bottom). Among all cell classes, only dimming detectors showed a significant increase in the number of spike discharges ($P < 0.05$, t-test, $n = 7$ cells; **Fig. 2d**, left) and a significant decrease in the oscillation index (see Methods; $P < 0.01$, t-test, $n = 7$ cells; **Fig. 2d**, right) in response to bicuculline. Thus, behavioral changes induced by intraocular injection of bicuculline may not be ascribed to changes in the activity of cell classes other than dimming detectors.

Applying a planar multi-electrode array to the isolated retinas[29], we closely examined the effects of bicuculline on the activities of dimming detectors. We mapped each receptive field center of recorded dimming detectors using a small flashing spot (**Fig. 3a**). Then we projected a dark spot that expanded from 0° (0 s) to 60° (1.4 s) on the retina (**Fig. 3a**,**b**). **Figure 3c** (top) illustrates an example of the spike trains simultaneously recorded from seven dimming detectors during a single presentation of the expanding dark spot. In the control condition, when the spot diameter exceeded ~40° (~0.9 s after stimulus onset), the inter-spike intervals became regular, and spike discharges were phase-locked across dimming detectors. Notably, for each dimming detector the latency of the first spike as well as the emergence of regular inter-spike intervals after the start of dark spot expansion varied from trial to trial (**Supplementary Fig. 2**). A PSTH (50-ms bin width) was constructed from the simultaneous spike trains recorded from seven dimming detectors during the single stimulus presentation (**Fig. 3c**). The number of spikes/bin increased as the dark spot expanded. The profile of PSTH seemed similar before (**Fig. 3c**) and during application of bicuculline (**Fig. 3d**). However, the regularity of

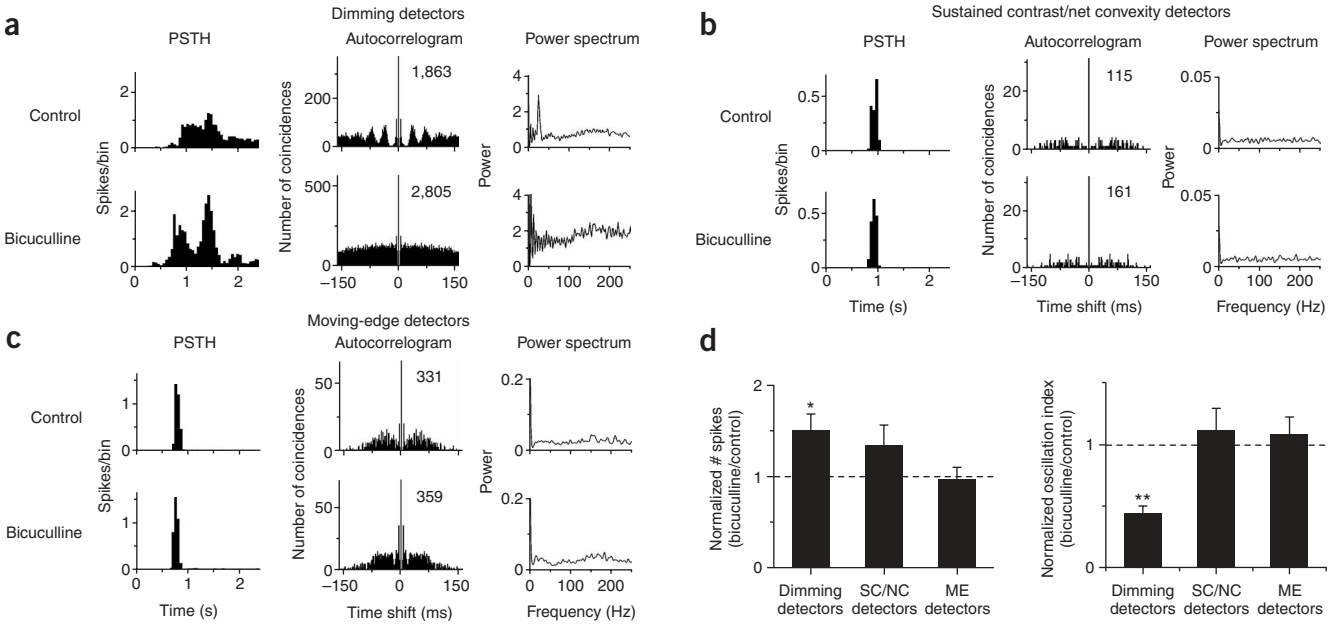

Figure 2 Effects of bicuculline on the activities of retinal ganglion cells. (**a**–**c**) Spikes were recorded during 100 repetitive trials from dimming detectors (**a**), sustained contrast and/or net convexity detectors (**b**), and moving-edge detectors (**c**). The dark spot expanded from 0° (0 s) to 60° (1.4 s) at the speed of 43° s^{-1} and then was maintained for 3 s. The PSTHs (left; 50-ms bin width), autocorrelograms (middle; 2-ms bin width) and power spectra (right) were calculated before (control) and during application of 10 μM bicuculline. In this and the following figures, the number shown in each autocorrelogram indicates the peak value at zero time shift. (**d**) Summary of the effects of bicuculline on the number of spikes (left) and the oscillation index (right). Mean ± s.e.m. Data obtained from seven dimming detectors, six sustained contrast and/or net convexity detectors (SC/NC detectors), and seven moving-edge detectors (ME detectors). $*P < 0.05$, $**P < 0.01$.

inter-spike intervals (**Fig. 3c**, top) seemed to be obscured by bicuculline (**Fig. 3d**, top).

To analyze the temporal pattern of spike trains, we created an ensemble spike train from the simultaneous spike trains recorded from several dimming detectors during repetitive presentations of the expanding dark spot. In the control condition, an autocorrelogram of the ensemble spike train showed a pattern with periodic peaks at regular intervals (**Fig. 4a**, left), and the power spectrum of the autocorrelation function showed a clear peak at ~40 Hz (**Fig. 4a**, right). Because the response period of each dimming detector was mostly overlapping during each stimulus presentation (**Fig. 3c**, top), these results indicate that the γ-range oscillations of each dimming detector (see **Fig. 2a**, control autocorrelogram and power spectrum) were phase-locked or synchronized. To demonstrate the synchrony of oscillations plainly, we extracted a synchronized event (**Fig. 4b**, top) where spikes were generated within 2 ms in multiple (≥2) dimming detectors (**Fig. 4b**, inset), and we calculated the autocorrelation (**Fig. 4b**, bottom left) and power spectrum (**Fig. 4b**, bottom right) from the synchronized event train.

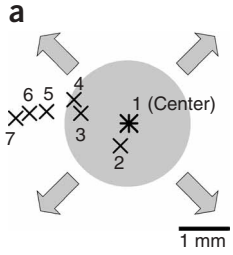

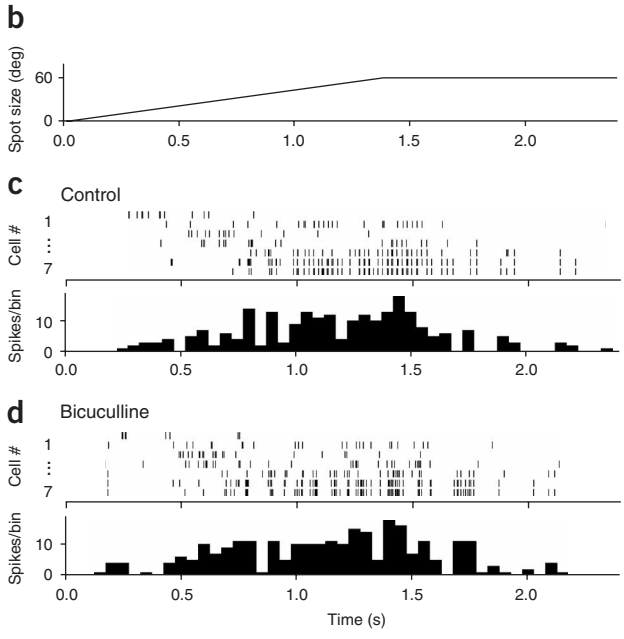

Figure 3 Spike trains evoked by an expanding dark spot in multiple dimming detectors in the isolated retina. (**a**) Map of receptive field centers of the seven recorded dimming detectors. The dark spot started expanding from the receptive field center of cell #1. Scale bar indicates 1.0 mm, which corresponds to ~10° of subtense. (**b**) Changes in spot size (diameter) with time. (**c**) A single-trial record of simultaneous spike trains in the control condition. Top: the raster plots of discharges simultaneously recorded from seven cells shown in **a**. Bottom: the peri-stimulus time histogram (PSTH, 50-ms bin width) calculated from the simultaneous spike trains shown above. (**d**) The raster plots (top) and PSTH (bottom) obtained from the same cells in the presence of 10 μM bicuculline.

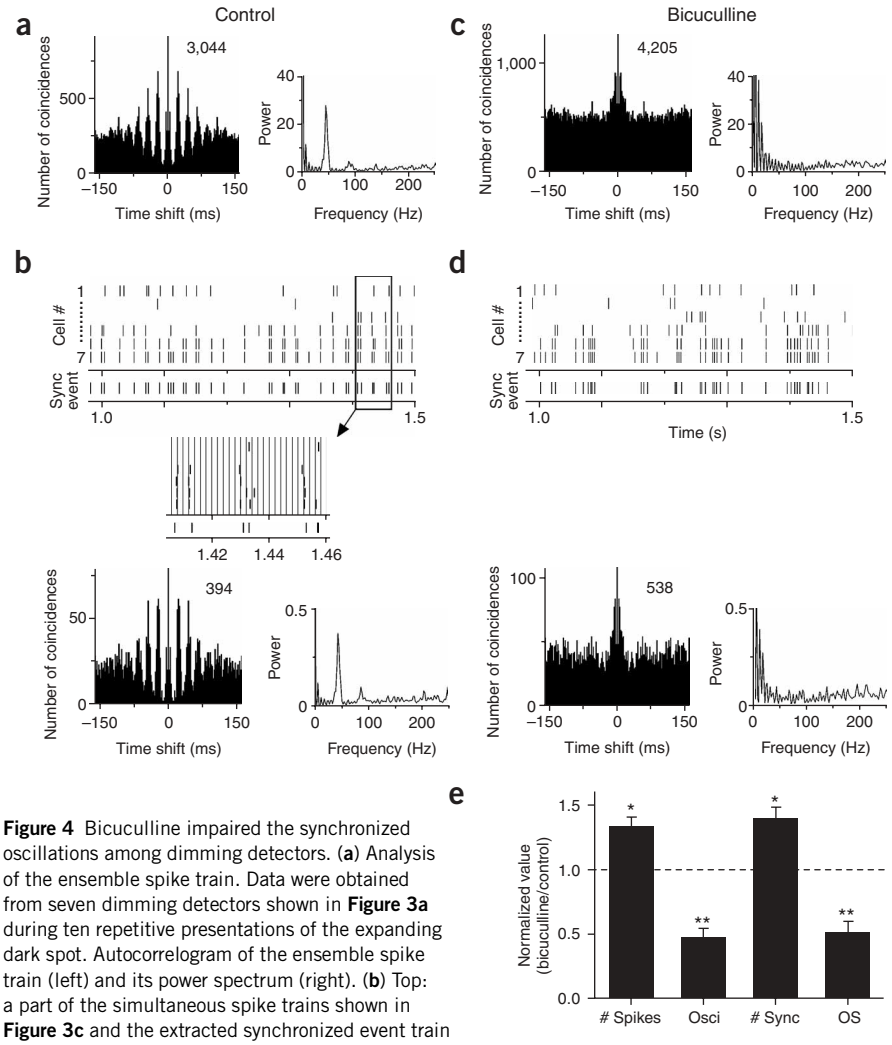

Figure 4 Bicuculline impaired the synchronized oscillations among dimming detectors. (**a**) Analysis of the ensemble spike train. Data were obtained from seven dimming detectors shown in **Figure 3a** during ten repetitive presentations of the expanding dark spot. Autocorrelogram of the ensemble spike train (left) and its power spectrum (right). (**b**) Top: a part of the simultaneous spike trains shown in **Figure 3c** and the extracted synchronized event train ('Sync event'). Inset, the simultaneous spike trains were grouped in 2-ms bins (vertical lines) and the synchronized events were extracted. Bottom: autocorrelogram of the synchronized event train (left) and its power spectrum (right). (**c**) Effects of bicuculline (10 μM) on the ensemble spike train. Autocorrelogram of the ensemble spike train (left) and its power spectrum (right). (**d**) Top: a part of the simultaneous spike trains in the presence of bicuculline shown in **Figure 3d** and the extracted synchronized events. Bottom: effects of bicuculline on the synchronized event train. Autocorrelogram of the synchronized event train (left) and its power spectrum (right). (**e**) Effects of bicuculline on the number of spikes ('# Spikes'), the oscillation index ('Osci'), the number of synchronized events ('# Sync'), and the oscillatory synchronization index ('OS'). Each value was normalized to the control condition. Mean ± s.e.m., $n = 5$ retinas. $^*P < 0.05$, $^{**}P < 0.01$.

These analyses indicate that the synchronized event occurred in oscillation (39.84 ± 3.36 Hz, $n = 5$ retinas).

Bicuculline impaired the oscillations (**Fig. 4c**) and the oscillatory synchronization (**Fig. 4d**). Periodic peaks disappeared both in the autocorrelogram calculated from the ensemble spike train (**Fig. 4c**, left) and in that from the synchronized event train (**Fig. 4d**, bottom left). In the power spectra there was no clear peak in the γ-range frequency (**Fig. 4c**, right and **4d**, bottom right). Note that under this condition both spikes and synchronized events were generated with random intervals because the number of coincidences in the autocorrelograms was almost constant besides the central peak (**Fig. 4c**, left and **4d**, bottom left).

Bicuculline significantly decreased both the oscillation index and the oscillatory synchronization index of dimming detectors ($P < 0.01$ for each; t-test, $n = 5$ retinas; **Fig. 4e**; see Methods). However, blockade of inhibitory interactions mediated by $GABA_A$Rs increased the number of spike discharges ($P < 0.05$), resulting in an increase in the number of synchronized events ($P < 0.05$). These results strongly suggest that the bicuculline-induced suppression of escape behavior (**Fig. 1d**) may be caused by impairment of the synchronized γ-range oscillations among dimming detectors.

To clarify the relationship between the synchronized oscillation and the distance between dimming detectors, we calculated cross-correlations for each pair of dimming detectors before and during application of bicuculline (**Fig. 5a**). In the control condition, cross-correlograms demonstrated a pattern with a central peak and periodic side peaks (**Fig. 5a**, top), indicating the presence of synchronization (the central peak) accompanied by oscillations (the side peaks). The shift predictors were almost flat (**Fig. 5a**, top, inset), indicating that the synchronization and oscillations had a neural origin. During bicuculline application the oscillations disappeared in all cell pairs (**Fig. 5a**). However, the synchronization still remained in near-cell pairs (0 to 0.5 mm; **Fig. 5a**) whereas it was obscured in remote-cell pairs (0.5 to 1 mm, and >1 mm; **Fig. 5a**). We found that during bicuculline application, the synchronization index (see Methods) did not change in near-cell pairs (0 to 0.5 mm, $n = 9$ pairs; **Fig. 5b**) but became significantly small in remote-cell pairs (0.5 to 1 mm, $n = 11$ pairs; >1 mm, $n = 49$ pairs; $P < 0.01$ each, t-test; **Fig. 5b**). These results suggest that suppression of oscillations by bicuculline may impair the long-range synchrony of spike discharges without affecting the local synchrony.

We also calculated time-resolved sliding-window cross-correlograms (200-ms time window, 20-ms sliding steps; see Methods) to examine how the synchronization and oscillations developed with increasing spot size (**Fig. 5c**, bottom). In the control condition, for both near- and remote-cell pairs, a clear striped pattern was observed along the time axis (> ~1 s), indicating the presence of synchronization (the horizontal center line at zero time shift) and oscillations (horizontal lines nearly parallel to the center line). With time the inter-stripe width became wider, suggesting that the frequency of oscillations decreased gradually. Bicuculline obscured the striped pattern in both pairs, indicating the suppression of oscillations. However, the center line (indicating synchronization) remained in the near-cell pair, whereas it disappeared in the remote-cell pair.

Potentiation of escape behavior by a $GABA_C$R antagonist

It is critical to know whether escape behavior is potentiated when retinal synchronized oscillatory activity is enhanced. We have already

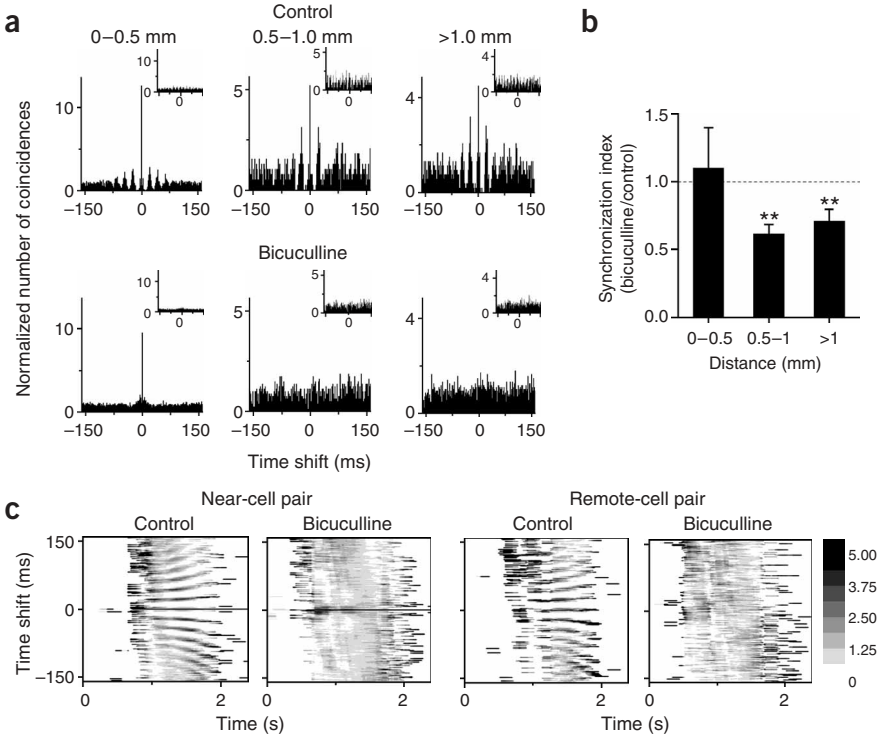

Figure 5 Effects of bicuculline on synchronization and oscillations. Cross-correlograms were calculated from spike discharges recorded from a pair of dimming detectors during ten repetitive presentations of the expanding dark spot. The spot size was increased from 0° (0 s) to 60° (1.4 s) at the speed of 43° s^{-1} and then was maintained for 3 s. (**a**) Examples of cross-correlograms and shift predictors (inset) obtained from three pairs of dimming detectors before (top) and during (bottom) application of bicuculline. Distance between receptive field centers of dimming detectors was categorized into three groups (top). (**b**) Distance-dependent suppression of the synchronization by bicuculline. The synchronization index in the presence of bicuculline was normalized to that in the control condition. Mean ± s.e.m., $n = 5$ retinas. $^{**}P < 0.01$. (**c**) Left: sliding-window cross-correlograms obtained from the near-cell pair shown in **a** (0–0.5 mm) before (Control) and during application of bicuculline. Right: sliding window cross-correlograms obtained from the remote-cell pair shown in **a** (>1.0 mm). The vertical and horizontal axes indicate time shift (ms) and the time course of stimulus presentation, respectively. Gray scale bar (right) indicates the number of coincidences normalized by the mean value of the corresponding shift predictor.

shown that the oscillations evoked by a large dimming stimulus in dimming detectors are enhanced by a $GABA_C$R antagonist, TPMPA[27]. It is probable that blockade of the $GABA_C$R-mediated negative feedback from amacrine cells to bipolar cells increases glutamate release from bipolar cells[30,31]. In contrast to injection of bicuculline, intraocular injection of TPMPA potentiated escape behavior in response to the expanding dark spot ($n = 5$ frogs) (**Fig. 6a**). Frogs responded to smaller dark spots with a higher escape rate ~2 h after TPMPA injection (**Fig. 6a**, filled squares) than in the control condition (**Fig. 6a**, open circles). The TPMPA-induced potentiation of escape behavior recovered 1 d after injection (**Fig. 6a**, open triangles). TPMPA shifted the relationship between the final spot diameter and the escape rate along the abscissa, suggesting that $GABA_C$Rs in the retina may contribute to controlling the sensitivity to escape behavior.

Effects of TPMPA on retinal ganglion cells

To examine the effects of TPMPA on the activities of retinal ganglion cells, we recorded spike discharges extracellularly from various cell classes within a retinal area that was stimulated by a dark spot expanding from 0° to 30°. TPMPA (10 μM) increased the number of spike discharges and enormously enhanced the γ-range oscillations in dimming detectors (**Fig. 6b**), whereas TPMPA did not change the profiles of PSTHs, autocorrelograms and power spectra in sustained contrast and/or net convexity detectors (**Fig. 6c**) or in moving-edge detectors (**Fig. 6d**). TPMPA induced a significant increase in the number of spike discharges and in the oscillation index only in dimming detectors ($P < 0.01$ each, t-test, $n = 6$ cells; **Fig. 6e**).

Applying a multi-electrode array to the isolated retinas, we simultaneously recorded the responses of several dimming detectors to a dark spot expanding from 0° to 30°, and we calculated autocorrelations from the ensemble spike train (**Fig. 7a**) and the synchronized event train (**Fig. 7b**). These analyses showed that TPMPA (10 μM) enhanced synchronized oscillatory activity. Power spectrum analysis indicated that TPMPA markedly increased the peak power of γ-range oscillations without changing their peak frequency (**Fig. 7a**,**b**). TPMPA significantly increased the oscillation index, the oscillatory synchronization index, the number of spike discharges and the occurrence of synchronized events in dimming detectors ($P < 0.05$ each, t-test, $n = 5$ retinas; **Fig. 7c**). Examination of these results and the bicuculline results (**Fig. 4**) suggests that the oscillation index and the oscillatory synchronization index seem to be good predictors of changes in escape behavior.

Effects of GABAR antagonists on optokinetic behavior

One may argue that GABAR antagonists might cause nonspecific disruption of retinal function. However, this seems unlikely. We examined the effects of GABAR antagonists on optokinetic responses to horizontally drifting stripes (**Fig. 8a**). Frogs pursued reciprocating motion of stripes by rotating their head. Approximately 2 h after intraocular injection of bicuculline, the frogs did not escape in response to the expanding dark spot (**Fig. 1d**), but the same frogs displayed optokinetic responses to the drifting stripes (**Fig. 8b**). The maximal angle of optokinetic head rotation did not change significantly ($P = 0.98$, repeated-measures ANOVA, $n = 5$ frogs). Furthermore, intraocular injection of TPMPA did not affect optokinetic responses ($P = 0.30$, repeated-measures ANOVA, $n = 5$ frogs; **Fig. 8c**). Therefore, the retinal system that was required to induce optokinetic responses was still functioning after the pharmacological treatments that markedly changed escape behavior.

DISCUSSION

In the present study, we examined the relationship between visually guided behavior and the activity of retinal ganglion cells in frogs. Intraocular injection of $GABA_A$R and $GABA_C$R antagonists caused suppression and potentiation of escape behavior, respectively, in response to an expanding dark spot (**Figs. 1d** and **6a**). The changes in escape behavior were not correlated with the discharge rate of ganglion cells but rather with changes in the synchronized oscillatory

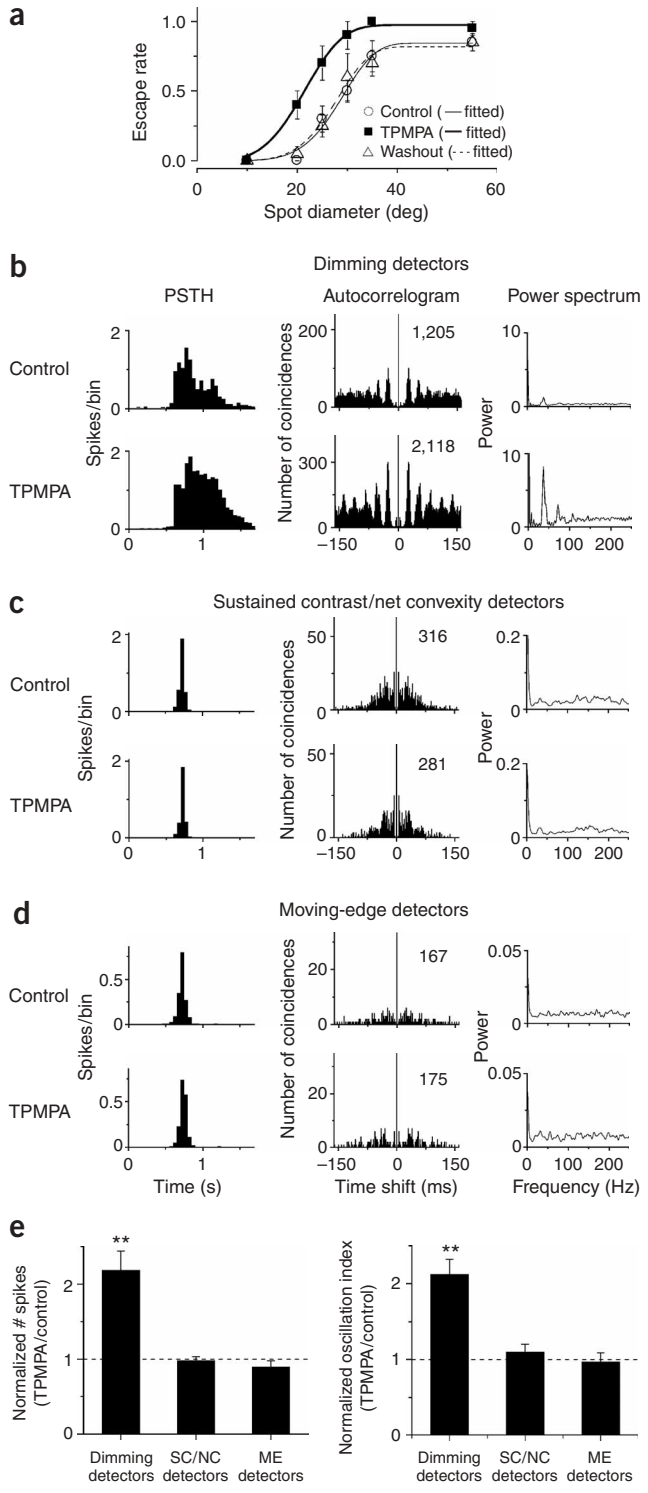

Figure 6 Effects of a $GABA_CR$ antagonist on escape behavior and the activities of retinal ganglion cells. (**a**) Relationship between the escape rate and the final spot diameter before (open circles), 2 h after (filled squares) and 1 d after (open triangles) intraocular injection of TPMPA. R^2 values of the Weibull function fitted to the data (solid and dotted lines) were 0.985 (control), 0.996 (TPMPA) and 0.985 (washout). (**b**–**d**) Effects of bath-applied TPMPA (10 μM) on the activities of dimming detectors (**b**), sustained contrast and/or net convexity detectors (**c**) and moving-edge detectors (**d**). The PSTHs (left; 50-ms bin width), autocorrelograms (middle; 2-ms bin width) and power spectra (right) were calculated from spikes that occurred during 100 repetitive presentations of the expanding dark spot (from 0° to 30° at an expansion speed of 43° s^{-1}). (**e**) Effects of TPMPA on the number of spikes (left) and the oscillation index (right). Mean ± s.e.m. Data were obtained from six dimming detectors, eight sustained contrast and/or net convexity detectors (SC/NC detectors) and four moving-edge detectors (ME detectors). $^{**}P < 0.01$.

activity of dimming detectors (**Figs. 2–7**). We also found that both the escape rate of frogs (**Fig. 1b**,**c**) and the oscillatory activities of dimming detectors (**Supplementary Fig. 3**) were similarly affected by the expansion speed and final diameter of the dark spot in the control condition (that is, without pharmacological treatment). Furthermore, escape behavior was strongly modified by the GABAR antagonists, whereas other behaviors, such as optokinetic responses to the drifting stripes, were not (**Fig. 8**). These results, therefore, suggest a strong tie between synchronized oscillatory activity among dimming detectors and escape behavior.

Although these results are strongly suggestive, they are not unequivocal. Proving that the synchronized oscillations in dimming detectors are responsible for escape behavior would require one of two things: (i) a demonstration that the GABAR antagonists we used to perturb escape behavior does not affect cell classes other than the dimming detector, or (ii) a demonstration that the dimming detector is the only cell class involved in this particular behavioral response. If the latter is the case, then effects of GABAR antagonists on other cell classes become irrelevant. It is difficult to prove either of these, and thus we have gathered substantial evidence in both directions.

First, we have shown that the firing patterns of the non-dimming detector classes were not changed by the GABAR antagonists (**Figs. 2** and **6**), as measured by changes in the profiles of the PSTHs, autocorrelograms and power spectra. (For this analysis we used firing patterns produced by an expanding dark spot, as this was the stimulus that evoked the escape behavior. However, this stimulus might not be optimal for detecting the effects of GABAR antagonists on the activities of the non-dimming detector classes because it has been reported that responses to bright light stimuli were modified by GABAR antagonists in frog retinal ganglion cells[32].) Second, we have shown that the firing patterns of the non-dimming detector classes were not as tightly linked to escape behavior as the firing patterns of dimming detectors. The non-dimming detector classes generated significantly stronger transient responses to the expanding dark ring than to the expanding dark spot, but the former stimulus did not elicit escape behavior (**Supplementary Fig. 1**). However, in dimming detectors both the number of spike discharges and the oscillation index were significantly reduced for the expanding dark ring than for the expanding dark spot (**Supplementary Fig. 1**). Thus, the non-dimming detector classes may have some role in escape behavior, but it is likely to be a lesser role than that of dimming detectors, whose responses are tightly correlated with the expanding dark spot stimulus.

In remote pairs of dimming detectors bicuculline suppressed both oscillations and synchronization (**Fig. 5**). However, in nearby pairs of dimming detectors bicuculline suppressed the oscillations but did not impair synchronization, perhaps because adjacent dimming detectors may have received excitatory common inputs and/or electrically coupled inputs[26,27,33]. The synchrony of spike discharges that occurred randomly in multiple local regions would be insufficient to evoke escape behavior. The γ-range oscillations may serve to adjust the local synchronizations in phase and to establish the synchronization between dimming detectors widely across the retina[26,34]. The long-range lateral

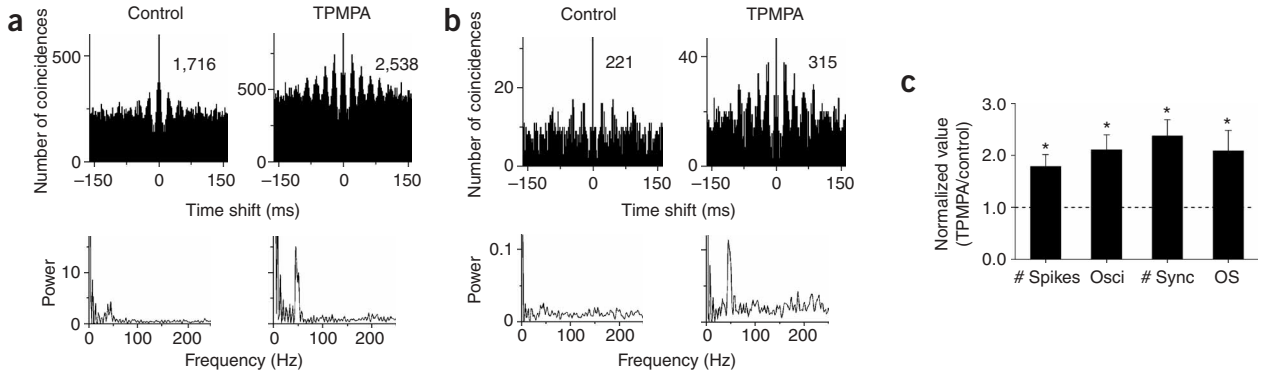

Figure 7 TPMPA enhanced the synchronized oscillatory activity among dimming detectors. Autocorrelograms were calculated from spike discharges recorded during ten repetitive presentations of the expanding dark spot (from 0° to 30° at the expansion speed of 43° s^{-1}). (**a**) Enhancement of the oscillations by bath-applied TPMPA (10 μM). Analysis of the ensemble spike train obtained from seven simultaneously recorded dimming detectors before (control) and during application of TPMPA as shown by autocorrelograms (top) and power spectra (bottom). (**b**) Enhancement of the oscillatory synchronization by TPMPA. Analysis of the synchronized event train before (Control) and during application of TPMPA as shown by autocorrelograms (top) and power spectra (bottom). (**c**) Effects of TPMPA on the number of spikes ('# Spikes'), the oscillation index ('Osci'), the number of synchronized events ('# Sync') and the oscillatory synchronization index ('OS'). Each value was normalized to that in the control condition. Mean ± s.e.m., $n = 5$ retinas. $^*P < 0.05$.

interactions between dimming detectors may be mediated by Na^+ spikes because blockade of Na^+ channels by tetrodotoxin suppresses oscillatory synaptic inputs to dimming detectors[27].

Na^+ spikes trigger the release of GABA from amacrine cells[35,36], and thus GABAergic amacrine cells may be important in the network that generates oscillations in the inner retina. Oscillatory activity among dimming detectors was suppressed by bicuculline, an antagonist specific to $GABA_A$Rs, whereas this activity was enhanced by TPMPA, an antagonist specific to $GABA_C$Rs. Both GABARs exist in the inner plexiform layer[37–39]. $GABA_C$Rs are expressed mostly at the axon terminals of bipolar cells[39]. It has been suggested that the $GABA_C$R-mediated negative feedback from amacrine cells to bipolar cells may be used to control the gain of glutamatergic transmission[30,31]. Therefore, blockade of $GABA_C$Rs may increase the release of glutamate from bipolar cells and enhance the direct excitatory input to dimming detectors and/or the inhibitory activity of amacrine cells, resulting in enhancement of the oscillatory activities of dimming detectors. When picrotoxin, which blocks both $GABA_A$Rs and $GABA_C$Rs in the frog retina[38], is applied, the oscillatory activity of dimming detectors is suppressed[26]. It is likely that $GABA_A$Rs may be essential for generating the oscillatory activities in the inner retina, whereas $GABA_C$Rs may have a different role, such as gain control. After blockade of $GABA_C$Rs, frogs show escape behavior in response to small spots that elicit little or no escape behavior under control condition (**Fig. 6a**). Activation of $GABA_C$Rs in the retina may attenuate the oscillatory activity of dimming detectors and may optimize the stimulus size tuning for eliciting escape behavior. Such adjustment may be useful to avoid unnecessary escape from tiny prey or a distant predator.

Synchronized oscillations among dimming detectors in a wide retinal area seems to convey essential escape-related visual information to the frog's brain. However, it is not evident which aspect of this activity is analyzed by central visual neurons such as neurons in the tectum[40]. There may be at least three possibilities: (i) synchronization, (ii) synchronization accompanied by γ-range oscillations and (iii) γ-range oscillations. In the first case, central visual neurons may behave as coincidence detectors. These neurons respond only to synchrony of discharges from many dimming detectors without taking into account oscillations. The function of oscillations may be limited only to establishing the synchronization of discharges among dimming detectors widely across the retina. Coincidence detection with a narrow time window may improve both noise tolerance and input discriminability[41–43]. In the second case, central visual neurons may fire only when synchronized events arrive repetitively at regular (~20 to ~30 ms) intervals. Such a mechanism may improve input discriminability and prevent false alarms. However, the probability of falling victim to predators would increase if central neurons responded only after the arrival of a large number of synchronized events at periodic intervals. A few synchronized events should trigger spikes in central neurons to elicit escape behavior. In the third case, central neurons may be tuned to a specific frequency of γ-range oscillations. These neurons would be

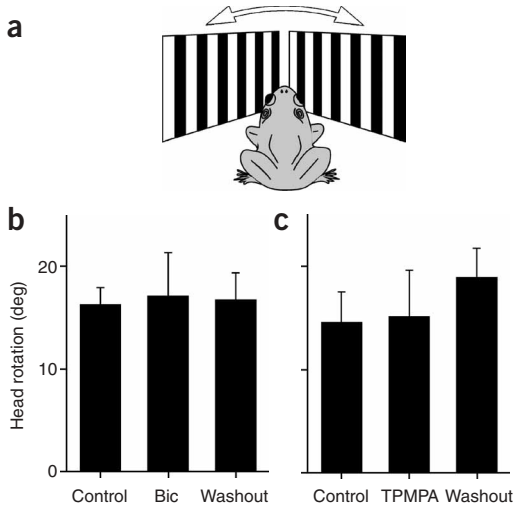

Figure 8 Effects of GABAR antagonists on optokinetic responses. (**a**) Horizontally drifting stripes (square wave) were presented on two displays in front of a frog. (**b**) The maximum angle of head rotation before (Control), 2 h after ('Bic') and 1 d after (Washout) intraocular injection of bicuculline (mean ± s.e.m., $n = 5$ frogs). (**c**) The maximum angle of head rotation before (Control), 2 h after (TPMPA) and 1 d after (Washout) intraocular injection of TPMPA (mean ± s.e.m., $n = 5$ frogs).

activated strongly if the frequency of postsynaptic potentials evoked by retinal inputs fit their resonance frequency[44], which would be determined by their intrinsic membrane properties or by a neuronal network. Further experiments are required to elucidate how the frog's brain decodes the synchronized retinal oscillations.

METHODS

Bullfrogs (*Rana catesbeiana*) were used for behavioral and electrophysiological experiments in accordance with the guidelines for the care and use of animals (The University of Tokyo and The Physiological Society of Japan).

Intraocular injection and behavioral experiments. Frogs were deeply anesthetized with ethyl 3-aminobenzoate methanesulfonate (3 g/l; MS-222, Sigma) before intraocular injection of GABA receptor antagonists. Bicuculline or TPMPA (500 μM; both from Tocris) dissolved in the standard solution (see 'Electrophysiology') was intravitreously injected into both eyes by a syringe (60 μl/eye). The final drug concentration in each eye was estimated to be ~50 μM. After sufficient recovery from anesthesia, we started behavioral experiments (~2 h after injection). To evaluate experimental artifacts, the standard solution without GABAR antagonists was injected into both eyes of a different group of frogs with the same protocol. Behavioral experiments were performed in a dark box (65 × 72 × 75 cm), and behavior of a frog placed in a transparent acrylic dome (30 cm in diameter) was monitored by a video camera under infrared illumination. For the test of escape behavior, a liquid crystal display (LCD, NANAO) was positioned 28.5 cm away from either eye (+135° (right eye) or −135° (left eye) from the median plane, 45° elevation from the horizontal; the plane of LCD was slanted off the horizontal), and an expanding dark spot (stimulus contrast, spot:background = 1:17) was presented (**Fig. 1a**). When the final spot diameter was changed, the spot diameter was increased from 0° to a final size (10° to 55° of subtense) at the speed of 43° s^{-1} and then maintained for 1 s during each trial. When the expansion speed was changed in the range between 5° s^{-1} and 50° s^{-1}, the final spot diameter was fixed to 55°. Two sessions were performed under each condition (**Fig. 1b**: eight trials per session, **Figs. 1c** and **6a**: 12 trials per session, **Fig. 1d,e**: six trials per session). To prevent habituation, a >60-s pause was inserted between trials and a 15-min pause between sessions, and the stimulus was presented alternately to each eye. The escape rate under each condition was the ratio of the number of trials where escape behavior was elicited to the total number of trials. The relationship between the spot diameter and the escape rate could be fitted with Weibull function by the Levenberg-Marquardt algorithm using Origin (OriginLab) software (**Fig. 6a**). For the test of optokinetic head rotation, two LCDs (Mitsubishi Electronics) were positioned in front of a frog (**Fig. 8a**). Vertical stripes (contrast = 0.89; spatial frequency of the square wave 0.1 cycles/degree, 50% duty cycle) were moved horizontally at a sinusoidally modulated speed (0.067 Hz, maximum speed +16° s^{-1} (right), −16° s^{-1} (left)). The reciprocating motion of the vertical stripes was presented for two cycles per trial, and three trials were performed under each condition. The maximum angle of head rotation in three trials was measured from digital video images with Matlab (Mathworks) software.

Electrophysiology. Experimental procedures and equipment has been described previously in detail[26]. Briefly, under a dim red light, a frog was double pithed and eyes were enucleated. The eyeball was hemisected, and the cornea and lens were separated from the posterior part. The eyecup was cut into several pieces and the retina was isolated carefully from the pigment epithelium. The isolated retina was transferred onto a planar multi-electrode array with the ganglion cell layer facing down and was superfused with a standard solution. The standard solution contained (in mM) 100.0 NaCl, 2.5 KCl, 1.6 $MgCl_2$, 1.0 $CaCl_2$, 18.0 $NaHCO_3$ and 10.0 D-glucose and was bubbled with 95% O_2/5% CO_2. To hold the ganglion cell bodies near the electrode surface, a Teflon ring frame holding a tightly stretched sheet of transparent dialysis membrane (50-kDa exclusion limit) was inserted into the recording chamber over the retina. Bicuculline (10 μM) or TPMPA (10 μM) was dissolved in the standard solution and bath-applied. Light-evoked spike discharges from ganglion cells were picked up by a multi-electrode array (8 × 8 array, electrode size 50 × 50 μm, interpolar distance 300 μm, MED-P5305, Alpha MED Sciences). The signals were amplified by a multi-channel differential amplifier and stored on a digital audio tape at a 24-kHz sampling rate. The spikes originating from an arbitrary ganglion cell were sorted by the template-matching technique[26]. Light stimuli presented on a cathode-ray tube display (Iiyama) were projected onto the retina through optics. Parameters of light stimuli used for electrophysiological experiments were similar to those for behavioral experiments. Using a laser beam, we confirmed experimentally that 10° of subtense corresponded to ~1.0 mm on the retina. Each time we used a new piece of isolated retina, we first examined receptive field positions and cell types from light-evoked spike discharges based on a previously described method[45].

Spike analyses. After spike sorting, peri-stimulus time histograms (PSTHs) were constructed, and auto- and cross-correlations were calculated with a bin width of 2 ms in a ±160 ms range. Shift predictors were computed to evaluate correlations from stimulus-locked coordination. The pattern of shift predictors was almost flat in all cases (**Fig. 5a**, inset). To investigate the temporal profile of spike trains simultaneously recorded from multiple ganglion cells, an ensemble spike train was created by superimposing the simultaneous spike trains. The strength of oscillations was assessed from the power spectrum, which was the fast Fourier transform (FFT) of the autocorrelogram calculated from the ensemble spike train. An oscillation index was defined as the ratio of the peak power in the γ range (20 to 60 Hz) to the mean power between 150 and 250 Hz in the power spectrum, because the power spectrum showed no peaks beyond 150 Hz[46] (**Figs. 2**,**4**,**6** and **7**). We extracted the synchronized event where spikes were generated within 2 ms in multiple (≥2) dimming detectors and created the synchronized event train. The occurrence time of the synchronized event was defined as the center of the bin that included multiple spikes. The autocorrelogram and power spectrum were calculated from the synchronized event train. An oscillatory synchronization index was defined as the peak power in the γ range to the mean power between 150 and 250 Hz in the power spectrum. A synchronization index was defined as the ratio of the number of coincidences at zero time shift in the raw cross-correlogram to the mean value of the shift predictor (±160 ms) for each cell pair. In time-resolved sliding-window cross-correlograms, the number of coincidences of the raw cross-correlogram for each window (200-ms width) was normalized to the mean number of coincidences of the shift predictor for the corresponding window to avoid the effect of changes in discharge rate, and the window was moved in 20-ms steps.

Note: Supplementary information is available on the Nature Neuroscience website.

ACKNOWLEDGMENTS

We thank L.H. Pinto, T. Takahashi, I. Arai and J. Hasegawa for discussion and comments and Y. Horiuchi for excellent technical assistance. This work was supported by Grant-in-Aid for Scientific Research (12053212 and 17022014 to M.T., 14710040 and 17730424 to H.I., 1610444 to M.G.) and the Special Coordination Funds for Promoting Science and Technology (The Neuroinformatics Research in Vision Project to M.T.) from the Ministry of Education, Science, Sports and Culture. M.G. is a research fellow of the Japan Society for Promotion of Science.

COMPETING INTERESTS STATEMENT

The authors declare that they have no competing financial interests.

Received 3 March; accepted 8 June 2005
Published online at http://www.nature.com/natureneuroscience/

1. Eckhorn, R. *et al.* Coherent oscillations: a mechanism of feature linking in the visual cortex? Multiple electrode and correlation analyses in the cat. *Biol. Cybern.* **60**, 121–130 (1988).
2. Gray, C.M., König, P., Engel, A.K. & Singer, W. Oscillatory responses in cat visual cortex exhibit inter-columnar synchronization which reflects global stimulus properties. *Nature* **338**, 334–337 (1989).
3. Wehr, M. & Laurent, G. Odour encoding by temporal sequences of firing in oscillating neural assemblies. *Nature* **384**, 162–166 (1996).
4. Fries, P., Roelfsema, P.R., Engel, A.K., König, P. & Singer, W. Synchronization of oscillatory responses in visual cortex correlates with perception in interocular rivalry. *Proc. Natl. Acad. Sci. USA* **94**, 12699–12704 (1997).
5. Stopfer, M., Bhagavan, S., Smith, B.H. & Laurent, G. Impaired odour discrimination on desynchronization of odour-encoding neural assemblies. *Nature* **390**, 70–74 (1997).

6. Laurent, G. A systems perspective on early olfactory coding. *Science* **286**, 723–728 (1999).
7. Rodriguez, E. *et al.* Perception's shadow: long-distance synchronization of human brain activity. *Nature* **397**, 430–433 (1999).
8. Castelo-Branco, M., Goebel, R., Neuenschwander, S. & Singer, W. Neural synchrony correlates with surface segregation rules. *Nature* **405**, 685–689 (2000).
9. Patel, A.D. & Balaban, E. Temporal patterns of human cortical activity reflect tone sequence structure. *Nature* **404**, 80–84 (2000).
10. Engel, A.K., Fries, P. & Singer, W. Dynamic predictions: oscillations and synchrony in top-down processing. *Nat. Rev. Neurosci.* **2**, 704–716 (2001).
11. Engel, A.K. & Singer, W. Temporal binding and the neural correlates of sensory awareness. *Trends Cogn. Sci.* **5**, 16–25 (2001).
12. Fell, J. *et al.* Human memory formation is accompanied by rhinal-hippocampal coupling and decoupling. *Nat. Neurosci.* **4**, 1259–1264 (2001).
13. Fries, P., Reynolds, J.H., Rorie, A.E. & Desimone, R. Modulation of oscillatory neuronal synchronization by selective visual attention. *Science* **291**, 1560–1563 (2001).
14. Neuenschwander, S. & Singer, W. Long-range synchronization of oscillatory light responses in the cat retina and lateral geniculate nucleus. *Nature* **379**, 728–733 (1996).
15. Castelo-Branco, M., Neuenschwander, S. & Singer, W. Synchronization of visual responses between the cortex, lateral geniculate nucleus, and retina in the anesthetized cat. *J. Neurosci.* **18**, 6395–6410 (1998).
16. Gray, C.M. & Singer, W. Stimulus-specific neuronal oscillations in orientation columns of cat visual cortex. *Proc. Natl. Acad. Sci. USA* **86**, 1698–1702 (1989).
17. Engel, A.K., Kreiter, A.K., König, P. & Singer, W. Synchronization of oscillatory neuronal responses between striate and extrastriate visual cortical areas of the cat. *Proc. Natl. Acad. Sci. USA* **88**, 6048–6052 (1991).
18. Engel, A.K., König, P., Kreiter, A.K. & Singer, W. Interhemispheric synchronization of oscillatory neuronal responses in cat visual cortex. *Science* **252**, 1177–1179 (1991).
19. Engel, A.K., König, P. & Singer, W. Direct physiological evidence for scene segmentation by temporal coding. *Proc. Natl. Acad. Sci. USA* **88**, 9136–9140 (1991).
20. Kreiter, A.K. & Singer, W. Stimulus-dependent synchronization of neuronal responses in the visual cortex of the awake macaque monkey. *J. Neurosci.* **16**, 2381–2396 (1996).
21. Engel, A.K., König, P., Kreiter, A.K., Schillen, T.B. & Singer, W. Temporal coding in the visual cortex: new vistas on integration in the nervous system. *Trends Neurosci.* **15**, 218–226 (1992).
22. Singer, W. & Gray, C.M. Visual feature integration and the temporal correlation hypothesis. *Annu. Rev. Neurosci.* **18**, 555–586 (1995).
23. Waldeck, R.F. & Gruberg, E.R. Studies on the optic chiasm of the leopard frog. I. Selective loss of visually elicited avoidance behavior after optic chiasm hemisection. *Brain Behav. Evol.* **46**, 84–94 (1995).
24. King, J.G., Lettvin, J.Y. & Gruberg, E.R. Selective, unilateral, reversible loss of behavioral responses to looming stimuli after injection of tetrodotoxin or cadmium chloride into the frog optic nerve. *Brain Res.* **841**, 20–26 (1999).
25. Lettvin, J.Y., Maturana, H.R., McCulloch, W.S. & Pitts, W.H. What the frog's eye tells the frog's brain. *Proc. Inst. Radio Eng.* **47**, 1940–1951 (1959).
26. Ishikane, H., Kawana, A. & Tachibana, M. Short- and long-range synchronous activities in dimming detectors of the frog retina. *Vis. Neurosci.* **16**, 1001–1014 (1999).
27. Arai, I., Yamada, Y., Asaka, T. & Tachibana, M. Light-evoked oscillatory discharges in retinal ganglion cells are generated by rhythmic synaptic inputs. *J. Neurophysiol.* **92**, 715–725 (2004).
28. Bäckström, A.C., Hemilä, S. & Reuter, T. Directional selectivity and colour coding in the frog retina. *Med. Biol.* **56**, 72–83 (1978).
29. Meister, M., Pine, J. & Baylor, D.A. Multi-neuronal signals from the retina: acquisition and analysis. *J. Neurosci. Methods* **51**, 95–106 (1994).
30. Dong, C.J. & Werblin, F.S. Temporal contrast enhancement via $GABA_C$ feedback at bipolar terminals in the tiger salamander retina. *J. Neurophysiol.* **79**, 2171–2180 (1998).
31. Matsui, K., Hasegawa, J. & Tachibana, M. Modulation of excitatory synaptic transmission by $GABA_C$ receptor-mediated feedback in the mouse inner retina. *J. Neurophysiol.* **86**, 2285–2298 (2001).
32. Bonaventure, N., Wioland, N. & Jardon, B. Anisotropic inhibition in the receptive field surround of the frog retinal ganglion cells, evidenced by bicuculline and SR 95103, a new GABA antagonist. *Eur. J. Pharmacol.* **121**, 327–336 (1986).
33. Brivanlou, I.H., Warland, D.K. & Meister, M. Mechanisms of concerted firing among retinal ganglion cells. *Neuron* **20**, 527–539 (1998).
34. König, P., Engel, A.K. & Singer, W. Relation between oscillatory activity and long-range synchronization in cat visual cortex. *Proc. Natl. Acad. Sci. USA* **92**, 290–294 (1995).
35. Watanabe, S., Koizumi, A., Matsunaga, S., Stocker, J.W. & Kaneko, A. GABA-Mediated inhibition between amacrine cells in the goldfish retina. *J. Neurophysiol.* **84**, 1826–1834 (2000).
36. Shields, C.R. & Lukasiewicz, P.D. Spike-dependent GABA inputs to bipolar cell axon terminals contribute to lateral inhibition of retinal ganglion cells. *J. Neurophysiol.* **89**, 2449–2458 (2003).
37. Wässle, H., Koulen, P., Brandstätter, J.H., Fletcher, E.L. & Becker, C.M. Glycine and GABA receptors in the mammalian retina. *Vision Res.* **38**, 1411–1430 (1998).
38. Du, J.L. & Yang, X.L. Subcellular localization and complements of $GABA_A$ and $GABA_C$ receptors on bullfrog retinal bipolar cells. *J. Neurophysiol.* **84**, 666–676 (2000).
39. Vitanova, L. *et al.* Immunocytochemical and electrophysiological characterization of GABA receptors in the frog and turtle retina. *Vision Res.* **41**, 691–704 (2001).
40. Grüsser, O.J. & Grüsser-Cornehls, U. Neurophysiology of the anuran visual system. in *Frog Neurobiology* (eds. Llinás, R. & Precht, W.) 297–385 (Springer, Berlin, 1976).
41. König, P., Engel, A.K. & Singer, W. Integrator or coincidence detector? The role of the cortical neuron revisited. *Trends Neurosci.* **19**, 130–137 (1996).
42. Salinas, E. & Sejnowski, T.J. Impact of correlated synaptic input on output firing rate and variability in simple neuronal models. *J. Neurosci.* **20**, 6193–6209 (2000).
43. Perez-Orive, J., Bazhenov, M. & Laurent, G. Intrinsic and circuit properties favor coincidence detection for decoding oscillatory input. *J. Neurosci.* **24**, 6037–6047 (2004).
44. Hutcheon, B. & Yarom, Y. Resonance, oscillation and the intrinsic frequency preferences of neurons. *Trends Neurosci.* **23**, 216–222 (2000).
45. Grüsser, O.J. & Grüsser-Cornehls, U. Comparative physiology of movement-detecting neuronal systems in lower vertebrates (Anura and Urodela). *Bibl. Ophthalmol.* **82**, 260–273 (1972).
46. Molotchnikoff, S., Shumikhina, S. & Moisan, L.E. Stimulus-dependent oscillations in the cat visual cortex: differences between bar and grating stimuli. *Brain Res.* **731**, 91–100 (1996).